Published online 24 May 2017

Nucleic Acids Research, 2017, Vol. 45, No. 13 ***7855–7869***
doi: 10.1093/nar/gkx480

Interlinked DNA nano-circles for measuring topoisomerase II activity at the level of single decatenation events

Emil L. Kristoffersen[1,2], Asger Givskov[1], Line A. Jørgensen[1], Pia W. Jensen[1], Jo Ann W. Byl[3], Neil Osheroff[3,4], Anni H. Andersen[1], Magnus Stougaard[5], Yi-Ping Ho[1,2,6,*] and Birgitta R. Knudsen[1,2,*]

[1]Department of Molecular Biology and Genetics, Aarhus University, 8000 Aarhus C, Denmark, [2]Interdisciplinary Nanoscience Center - iNANO, Aarhus University, 8000 Aarhus C, Denmark, [3]Department of Biochemistry, Vanderbilt University School of Medicine, Nashville, TN 37232, USA, [4]VA Tennessee Valley Healthcare System, Nashville, TN 37212, USA, [5]Department of Pathology, Aarhus University Hospital, 8000 Aarhus C, Denmark and [6]Division of Biomedical Engineering, Department of Electronic Engineering, The Chinese University of Hong Kong, Shatin, NT, Hong Kong SAR, China

Received April 04, 2017; Revised May 10, 2017; Editorial Decision May 15, 2017; Accepted May 22, 2017

ABSTRACT

DNA nano-structures present appealing new means for monitoring different molecules. Here, we demonstrate the assembly and utilization of a surface-attached double-stranded DNA catenane composed of two intact interlinked DNA nano-circles for specific and sensitive measurements of the life essential topoisomerase II (Topo II) enzyme activity. Topo II activity was detected via the numeric release of DNA nano-circles, which were visualized at the single-molecule level in a fluorescence microscope upon isothermal amplification and fluorescence labeling. The transition of each enzymatic reaction to a micrometer sized labeled product enabled quantitative detection of Topo II activity at the single decatenation event level rendering activity measurements in extracts from as few as five cells possible. Topo II activity is a suggested predictive marker in cancer therapy and, consequently, the described highly sensitive monitoring of Topo II activity may add considerably to the toolbox of individualized medicine where decisions are based on very sparse samples.

INTRODUCTION

Sensors and sensor systems made of DNA have gained increasing interest over the past several years. This is due in part to the recent advances in chemical synthesis of modified DNA oligonucleotides and to the ease by which DNA sensor systems can be combined with various DNA nanomaterials. Hence, various DNA sensors or sensor systems for the detection of small molecules (1–4), proteins (5,6), or even enzyme activities (6–10), based on optical or electrochemical readout, have been reported. Some of these have been successfully integrated with more complex nano-structures (11–14). Many of the sensors or sensor systems are built as relatively simple structures, exemplified by single- or double-stranded DNA structures containing Förster resonance energy transfer (FRET) pairs or DNA sequences that fold (or unfold) into DNAzyme or triplex structures upon external stimuli (2,9,15,16). More recently, a robust and fully reversible logic circuit was constructed by a more complex interlocked DNA nanostructure forming a double-stranded DNA pseudo-catenane (5).

Because DNA is easily amplified by naturally occurring polymerases, it is an excellent sensor material that can be used for sensitive detection of a broad variety of targets. The use of a rolling circle amplification (RCA) reaction to amplify DNA has been utilized for the detection of nucleotide sequences (17–23) as well as small molecules (24–27) that facilitate circularization of specific DNA molecules. The RCA reaction generates long tandem repeat DNA products that can be detected at the single–molecule level by a variety of visualization techniques, including cryo-transmission electron microscopy, atomic force microscopy or fluorescence microscopy (22,28–34). RCA-based techniques have also been demonstrated successful for amplification of signals generated from enzyme reactions, e.g. the cleavage-ligation reactions of the nuclear enzyme topoisomerase I (Topo I) from humans (30,35,36) or the malaria parasite *Plasmodium* (37,38). More recently, we reported specific and sensitive detection of the retroviral integrase (IN) activity by an

*To whom correspondence should be addressed. Tel: +45 6020 2673; Fax: +45 8619 6500; Email: brk@mbg.au.dk
Correspondence may also be addressed to Yi-Ping Ho. Tel: +852 3943 4340; Fax: +852 2603 5558; Email: ypho@ee.cuhk.edu.hk

RCA-based method (39). In these assays, based on rolling circle enhanced enzyme activity detection (REEAD), a specific DNA molecule (the REEAD substrate) is converted into a product composed of a DNA circle that can template a RCA-reaction. When primed in solution or by a surface attached DNA molecule, this product allows measurement of target enzymes at the single catalytic event level (30). Consistently, by combining REEAD with droplet microfluidics it was possible to detect enzymatic activity in single cells (35). Hence, REEAD has been demonstrated applicable as a sensitive and specific detection method for a broad array of biological or clinically important enzyme activities but has, until now, only been used to detect the relatively simple cleavage-ligation activities of type IB topoisomerases, recombinases and integrases (39,40). A highly attractive new target for REEAD is topoisomerase II (Topo II). However, the development of an assay for Topo II detection involves a completely new principle for substrate design, since Topo II, despite the kinship with Topo I in terms of cellular function, is an entirely different and phylogenetic unrelated enzyme with a different mechanism of action, a different structure and different utilization of cofactors (41). Indeed the complexity of the Topo II reaction mechanism has no resemblance with that of Topo I and the two enzymes share very little besides their names and their ability to relax DNA.

Human Topo II is of great importance in anti-cancer therapy and is the primary target of a large number of clinically used chemotherapeutics such as the drug etoposide (42–45). Unfortunately, a frequent side effect of treatment with these drugs is the development of resistance or secondary cancers (46–48). Besides its clinical relevance, Topo II is one of the important regulators of DNA topology in human cells (49). The enzyme functions as a protein homodimer and exerts its activity by introducing a transient staggered double-stranded break in the DNA. During this process, each subunit of the protein dimer becomes covalently attached to the DNA ends. Upon ATP binding, a conformational change in Topo II pulls the two ends of the cleaved DNA apart, which allows another DNA segment to pass through the generated opening before the enzyme religates the DNA break and dissociates from the DNA (43,50,51). All currently used Topo II-targeting anti-cancer drugs act by inhibiting the religation reaction of Topo II (43). Thereby, they turn Topo II into a cellular toxin, as the generated DNA breaks can lead to genome fragmentation and ultimately cell death (43). This mechanism of action of Topo II-targeting drugs points toward a direct correlation between Topo II activity and chemo-response in human cells. Consistently, the available evidence suggests a potential correlation between Topo II expression and drug response, at least in some cancers (52–56). However, due to the lack of sensitive and reliable methods for measurements of Topo II activity directly in samples with a small number of cells such as biopsies or primary cell cultures, the current evidence is based on a measure of gene-copy number, or the expression at the mRNA or protein levels (52–56). Unfortunately, the amount of protein expressed represents only one of several potential effectors of enzyme activity, which can also be affected by regulation mechanisms such as post-translational chemical modifications and/or by interactions with other proteins. Hence, the availability of sensor systems for measuring Topo II activity directly in human cancers may be of great value for elucidating a potential correlation between Topo II activity and chemo-response.

In the current study, we describe the programmed assembly of a surface-attached nanostructure consisting of two interlinked double-stranded DNA circles and the use of such structure for specific and sensitive RCA-enhanced detection of Topo II activity. Using this method, Topo II activity was monitored by the release of interlinked DNA circles from the surface. After specific nicking followed by RCA and hybridization of the RCA products (RCPs) with molecular beacons containing fluorophore-quencher pairs, each released circle could be detected at the single-molecule level by fluorescence microscopy or in bulk solution using a fluorescence reader. Because the protocol involved only isothermal amplification, the method was directly quantitative in nature. Moreover, because each RCP was the result of a single decatenation event mediated by Topo II, the method allowed direct quantification of Topo II activity at the single catalytic event level. Consistently, the REEAD assay allowed quantitative detection of purified Topo II as well as Topo II in human cell extracts consisting of approximately five to 5000 cells. As demonstrated by depletion experiments, the assay was specific for Topo II activity. Finally, we were able to demonstrate multiplexed detection of Topo II and Topo I of which the latter is also an important target for anti-cancer treatment.

MATERIALS AND METHODS

Enzymes and reagents

T4 polynucleotide kinase, T4 DNA ligase, Exonuclease I (ExoI), Exonuclease III (ExoIII), XbaI, Nt. BbvCI and BSA, were purchased from New England Biolabs. Unless stated otherwise, all chemicals were obtained from Sigma-Aldrich. ATP was purchased from Roche. γ-^{32}P-labeled ATP was purchased from PerkinElmer. MyOne™ Streptavidin C1 dynabeades and magnetic beads separation rack was purchased from Invitrogen. Gel mix (Ultra-pure SequaGel) for denaturing polyacrylamide gels was purchased from National Diagnostics. Complete, EDTA-free Protease inhibitor cocktail was purchased from Roche. k-DNA was purchased from TopoGen. All oligonucleotides were purchased from GeneLink.

Oligonucleotides

Other oligonucleotides. The sequence of the oligonucleotide used for the control circle was: 5′-GGA AGA GAT GGC GAC ATC ATC GAT CGG TCG GCA CCG GAT CCC TGC AGG CTG AGG ATA AGC GAT CTT CAC AGT TAC GAA CTG ACC TCA ATG CTG CTG CTG TAC TAC AGC TGA TCC TGA TGG-3′; and ligator oligonucleotide was: 5′-GTC GCC ATC TCT TCC CCA TCA GGA TCA GCT-3′.

The sequence of the REEAD substrate for Topo I, S(Topo I) was: 5′-AGA AAA ATT TTT AAA AAA CCC AAT AAG CGA TCT TCA CAG TCC CTT TTT TAA AAA TTT TTC TAA GTC TTT TAG ATC AAA CCT CAA TGC TGC TGC TGT ACT ACA AAG ATC TAA

AAG ACT TAG A-Amine-3′; The sequence of the primer for RCA of the S(hTopo I) circle was: 5′-ACT GTG AAG ATC GCT TAT-3′.

ID16 beacon: (2′OMe-RNA) 5′-CAL-Fluor-Red-590 (TAMRA analog)-GUA GAC CUC AAU GCU GCU GCU GUA CUA C-BHQ-2 (Black Hole Quencher-2)-3′.

ID33 beacon: (2′OMe-RNA) 5′-FAM-AGC CAC CUC AAU GCA CAU GUU UGG U-BHQ1 (Black Hole Quencher-1)-3′.

The sequence of the capture oligonucleotide used for coating microscopic slides and binding RCPs was: 5′-Amine-CCA ACC AAC CAA CCA AAT AAG CGA TCT TCA CAG T-3′.

The sequences of the oligonucleotides used to form the suicide substrate were: 5′-ATG AGC GCA TTG TTA GAT TTA CGA CAC CGG A (biotin)-3′ and 5′-AAT CTA ACA ATG CGC TCA TCG TCA TCC T-amine -3′.

Expression and purification of recombinant enzymes

Human topoisomerase I was expressed and purified essentially as described (8). Expression and purification of human Topoisomerase IIα (Topo IIα) was as described in (57). Expression and purification of human Topoisomerase IIβ (Topo IIβ) was performed as described in (58).

Preparation of nuclear cell extracts

Frozen pellets of 5×10^6 HeLa cells (unless stated otherwise in the text) were thawed on ice and incubated on ice for 10 min in lysis buffer (0.1% Igepal (CA-630), 10 mM Tris–HCl, pH 8, 20 mM $MgCl_2$ and 15 mM NaCl) (1 ml/2×10^6 cells) before centrifugation at 2200 rpm for 5 min. The supernatant was discarded and extraction buffer (0.5 M NaCl, 20 mM HEPES, pH 8, 20% v/v glycerol) (10 μl/10^6 cells) was added to the pellet followed by rotation of the sample for 1 h at 4°C. Finally, cell debris were precipitated by centrifugation at 11 000 rpm for 10 min and the supernatant recovered. Freshly prepared phenylmethylsulfonyl fluoride (PMSF) dissolved in isopropanol was added in all steps every 15 min (1/1000 of the total volume each time). Nuclear extracts were always freshly prepared and stored on ice for no more than 1 h before use.

Preparation of cellular extracts depleted of Topo II

Whole cell extracts used for Topo II depletion experiments were prepared by incubating frozen pellets of 10^6 HeLa cells with ice-cold low-osmotic lysis buffer [10 mM Tris–HCl, pH 7.5, 2 mM EDTA with Complete, EDTA-free protease inhibitor cocktail (50 μl buffer/10^6 cells)] for 10 min. Etoposide (100 μM, final concentration) or DMSO (the solvent of etoposide) and NaCl (300 mM, final concentration) were added and samples were incubated at room temperature for 10 min, followed by centrifugation at 11 000 rpm for 5 min at room temperature. Supernatants from the Topo II-depleted (containing etoposide) or non-depleted (containing DMSO) cell extracts were collected and the NaCl concentration was adjusted to 300 mM before use. As a negative control experiment, an aliquot of the non-depleted cell extract was heat inactivated by incubation at 95°C for 20 min. 1 μl cell extract (corresponding to extract from ∼15 000 cells) was used in the TADA experiments.

Preparation of the dsDNA catenane and other DNA substrates

The dsDNA catenane. All oligonucleotides used for assembling the A- and B-circle in the dsDNA catenane are listed in the Table 1. 25 pmol of each of the oligonucleotides were 5′-phosphorylated by 1 U/μl (final concentration) T4 polynucleotide kinase in a 5 μl reaction volume of 1× kinase buffer (70 mM Tris–HCl, pH 7.6, 10 mM $MgCl_2$, 1 mM ATP, 5 mM DTT), plus 5 mM KCl, and 5% glycerol (coming from the T4 kinase storage buffer) for 1 h at 37°C. 25 pmol (the total volume) of each of the phosphorylated oligonucleotides OL1, OL2 and OL3 of the A-circle were mixed in Tube 1 and ligated by incubation with T4 DNA ligase (16 U/μl, final concentration) for 30 min at room temperature. Following the same protocol as described for Tube 1, 25 pmol of each of the oligonucleotides OL8, OL9, and OL11 of the B-circle were ligated in Tube 2 (Step 1 in Figure 1A). After ligation, the content of Tubes 1 and 2 were transferred to a new tube (Tube 3) mixed and heated to 85°C for 1 min followed by incubation at room temperature for 5 min. Subsequently, T4 ligase (8 U/μl, final concentration) and fresh ATP (1 mM, final concentration) was added and incubation continued at room temperature for 1 h (described in Steps 2 and 3 of Figure 1A). Subsequently, 50 pmol of oligonucleotide OL12 were added to tube 3 and the reaction volume was adjusted to 210 μl with 1× T4 ligase buffer (50 mM Tris–HCl, pH 7.6, 10 mM $MgCl_2$, 1 mM ATP, 10 mM DTT). Then the reaction mixture was heated to 85°C and slowly cooled to room temperature over 1 h, before 50 pmol of each of the phosphorylated oligonucleotides OL4–OL7, OL10, OL13–OL16 (already stored in 1× kinase buffer) were added and incubation continued at room temperature overnight. T4 ligase (12 U/μl, final concentration) and 1 mM of fresh ATP were added to the reaction mixture, the volume adjusted to 300 μl of 1× T4 ligase buffer followed by incubation at 16°C for 2 h (Step 4, Figure 1A). Following ligation, the reaction volume was adjusted to 600 μl of the recommended buffer conditions for exonuclease digest (25 mM Tris–HCl, pH 7.6, 10 mM $MgCl_2$, 0.5 mM ATP, 5 mM DTT) and the mixture was incubated with ExoI (0.5 U/μl) and ExoIII (0.6 U/μl) for 1 h at 37°C (described in Step 5 of Figure 1A). Finally, the sample was heated to 70°C for 20 min and slowly cooled to room temperature before use. The dsDNA catenane was stored on ice for up to one week before use. The concentration of the generated dsDNA catenane was estimated to ∼4.5 nM (for a standard assembly) by quantification of the band representing dsDNA relative to the band representing a known concentration of OL8 after gel-electrophoretic analyses (data not shown).

Control circle. The oligonucleotides for the control circle were 5′-phosphorylated by T4 polynucleotide kinase using the reaction conditions recommended by the manufacturer. The 5′-phosphorylated control circle oligonucleotide was mixed with 10-fold excess of the ligator oligonucleotide and incubated for 1 h at room temperature with T4 DNA Ligase (4 U/μl) (the final concentration of the control circle

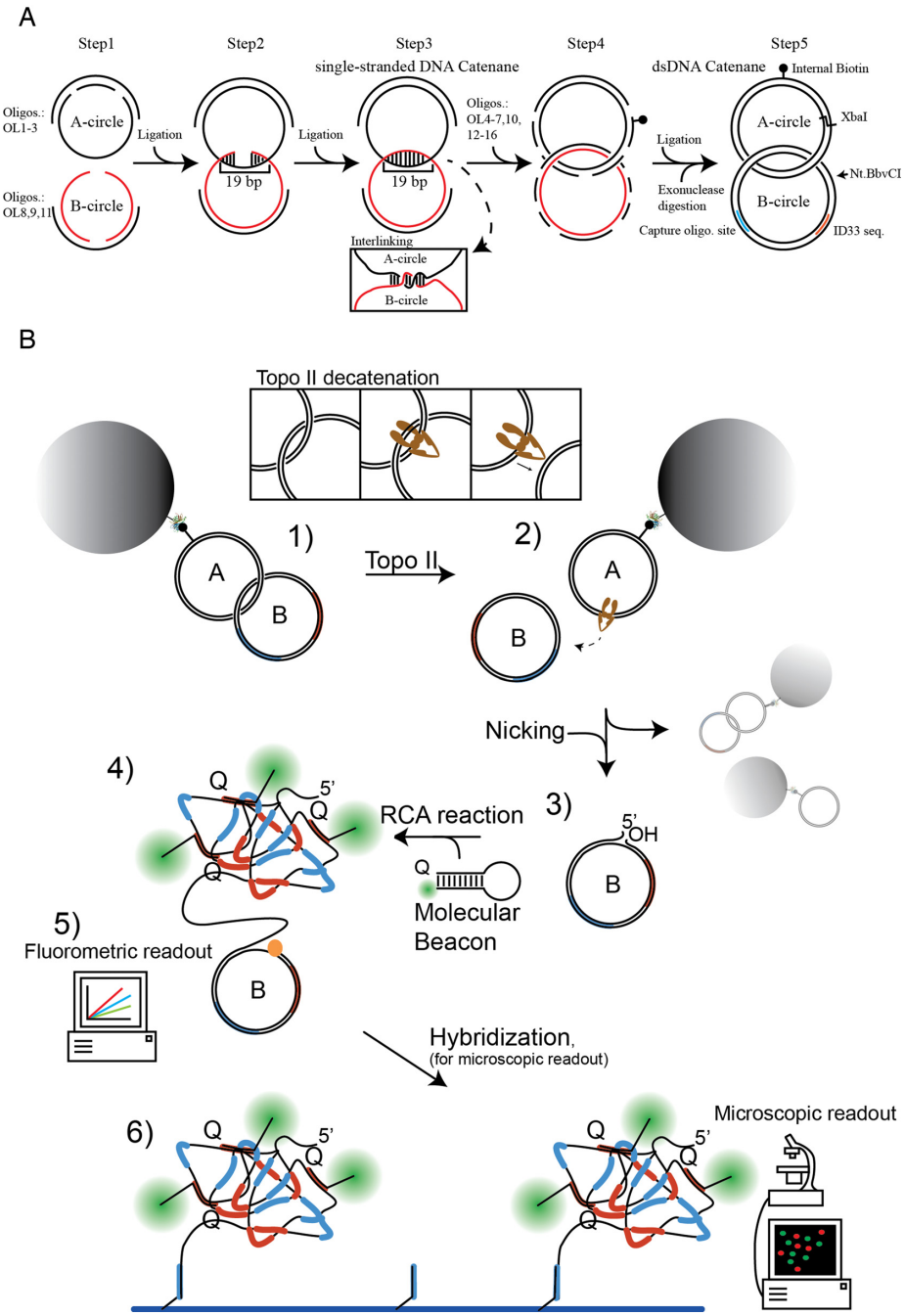

Figure 1. Outline of the TADA setup. (**A**) Step 1: To generate the 220 or 221 nt long oligonucleotides that constitute one strand of each of the double-stranded circles of the dsDNA catenane substrate, two parallel hybridization reactions were performed; one for the A-circle (with oligonucleotides OL1–OL3) and one for the B-circle (with oligonucleotides OL8, OL9 and OL11). Step 2: Addition of T4 DNA ligase followed by mixing of the two reaction products results in formation of the structure shown in Step 2. Here the B-circle hybridizes to the A-circle in a stretch of 19 bp. Step 3: Due to the double helical structure of duplex DNA, which has a periodicity of ∼10.5 bp/link, the ligation in Step 2 will result in interlinking of the A-circle and the B-circle. The resulting interlinked structure, termed the single-stranded DNA catenane, is shown in Step 3. The box illustrates the interlinked A- and B-circles with topological resolution. Step 4: After formation of the single-stranded DNA catenane, complementary oligonucleotides for the A-circle (OL4–OL7) and complementary oligonucleotides for the B-circle (OL10, OL12–OL16) were hybridized to the single-stranded DNA catenane. Step 5: The oligonucleotides were ligated to form the dsDNA catenane. The black circle illustrates a biotin that is internally attached to one of the complementary oligonucleotides. (**B**) Schematic illustration of the TADA work flow. 1) The dsDNA catenane was attached to streptavidin coated magnetic beads (depictured as gray sphere) via the biotin in the A-circle. (ii)2 Topo II (brown structure) decatenated the A-circle and the B-circle by the cleavage-ligation mechanism depictured in the inserted box. 3) The magnetic beads were precipitated, removing attached A-circles and unreacted catenanes from the solution. The decatenated B-circles that were recovered in the supernatant were nicked by the Nt.BbvCI nicking enzyme to create a 3′-OH end that could prime the RCA reaction. 4) The nicked B-circles were subjected to RCA in the presence of molecular beacons that hybridized to the RCPs, resulting in increased fluorescence due to separation of the quencher–fluorophore pair in the individual beacons. 5) The increase in fluorescence could be monitored directly in a fluorometer (the fluorometric readout). 6) RCPs with the bound molecular beacons could be immobilized on microscopic slides by hybridization to a capture oligonucleotide covalently attached to the slide and the results examined using a fluorescence microscope (the microscopic readout).

Table 1. TADA oligonucleotides

OL	Sequence (5′-3′)	Size, nt	Part of
1	CCGATGAGAAAGCGACTTACCGAATTCTCTAGAGAAGTTCCTATTCCGAAGTTCCTATTCTC TAGAAAGTATAGGAACTTCGTCATCTCTTCCCCATCAGGAATGAATAGGCAGAGAGACC	121	A
2	GGTCGGTACGACACCGGATCATGCGCGTGTGTAGCCGGTGACACGCTCATGACGCGATCA TG CGTGGACTGATCACTGTTCTAAGCTGTTAATGACCTAG	100	A
3	CGCTTTCTCATCGGCTAGGTCATTAACAGCTTAGAACAGTGATCAGTCCACGCATGATCGCG TCATGAGCGTGTCACCGGCTACACACGCGCATGATCCGGTGTCGTACCGACCGGTCTCTC TG	124	A
4	TATACTTTCTAGAGAATAGGAAC(*T-biotin*)TCGGAATAGGAACT	38	A
5	CCTATTCATTCCTGATGGG	19	A
6	GAAGAGATGACGAAGTTCC	19	A
7	TCTCTAGAGAATTCGGTAAGT	21	A
8	GGAAGAGATGGCGACATCATCGATCGGTCGGCACCGGATCCCTGCAGGCTGAGGATAAGC GATCTTCACAGTTACGAACTGACCTCAATGCACATGTTTGGCTCCAGCTGATGCTCATCG	120	B
9	GCTAAGCCAGGTGCACGCATGTCGATGTGTCGCAATCGCATGTTGTCATCGTGCATGCATCA TGACGTGCTGACGCGATGACTGAAGCTGATCCTGATGG	100	B
10	TCAGCACGTCATGATGCATGCACGATGACAACATGCGATTGCGACACATCGACATGCGTG CA	62	B
11	CCTGGCTTAGCCGATGAGCATCAGCTGGAGCCAAACATGTGCAT	44	B
12	GTCGCCATCTCTTCCCCATCAGGATCAGCTTCAGTCATCGCG	42	B
13	TGAGGTCAGTTCGTAACT	18	B
14	GTGAAGATCGCTTATCCT	18	B
15	CAGCCTGCAGGGATCCGG	18	B
16	TGCCGACCGATCGATGAT	18	B

oligonucleotide was 100 nM). Following ligation, the control circle was ready for RCA. The ligator oligonucleotide functioned as a primer to initiate the RCA.

Preparation of the TADA-complex

The TADA-complex was formed by mixing the dsDNA catenane (10 μl (45 fmol) per sample) with MyOne™ Streptavidin C1 dynabeads (50 μg per sample) followed by incubation at room temperature for 15 min. Subsequently, the TADA-complex was washed 5× in 1 ml of B&W buffer (5 mM Tris–HCl, pH 7.5, 0.5 mM EDTA, 1 M NaCl), 5× in 1 ml of 1× TE (10 mM Tris–HCl, pH 7.5, 0.5 mM EDTA) and 5× in 1 ml of Topo II decatenation buffer (10 mM Tris–HCl, pH 7.5, 10 mM $MgCl_2$, 0.5 mM EDTA, 15 μg/ml BSA, 100 mM KCl). All washing steps were performed at 42°C. Supernatants were removed after precipitating the beads on a magnetic beads separation rack for approximately 1 min. After the final washing step, the TADA-complex was moved to new tubes, precipitated and the supernatant was discarded. The precipitated complexes were now ready for use.

Endonuclease cleavage of the TADA-complex

The precipitated TADA-complex was re-dissolved in NEB cutsmart buffer (50 mM potassium acetate, 20 mM Tris-acetate pH 7.9, 10 mM magnesium acetate and 100 μg/ml BSA) and incubated with XbaI (2 U/μl, final concentration) and/or Nt. BbvCI (nicking endonuclease) (1 U/μl, final concentration) at 37°C for 1 h in a final volume of 10 μl. Subsequently, the beads and supernatant were separated by placing the reaction tubes in a magnetic beads separation rack followed by moving the supernatant liquid (potentially containing the released B-circles) to new tubes. The supernatant was analyzed by the fluorometric readout or the microscopic readout as described below.

Topo II decatenation measurement using TADA

The precipitated TADA-complex was re-dissolved in 1× Topo II decatenation buffer (10 mM Tris–HCl, pH 7.5, 10 mM $MgCl_2$, 0.5 mM EDTA, 15 μg/ml BSA, 100 mM KCl, 1mM ATP) and either purified Topo IIα, Topo IIβ or cell extract was added to the reaction tubes. Decatenation reactions were carried out for 30 min at 37°C in a total volume of 10 μl. Samples were then moved to the magnetic rack, the beads precipitated and the supernatant collected. The volume and the buffer composition of the supernatant was adjusted to 20 μl of 5 mM Tris–HCl, pH 7.5, 10 mM $MgCl_2$, 0.25 mM EDTA, 7 μg/ml BSA, 50 mM KCl before Nt.BbvCI nicking endonuclease (0.5 U/μl, final concentration) was added to the samples and incubation continued for 1 h at 37°C. Following nicking, the samples were ready for readout as described below.

Fluorometric readout

7.5 μl of samples containing released and nicked B-circle, prepared as described above, were moved to quantitative PCR (qPCR) tubes and the volume adjusted to 10 μl of 1× RCA buffer (33 mM Tris-acetate, pH 7.9, 10 mM $MgCl_2$, 66 mM KCl, 1% (v/v) Tween 20, and 10 mM DTT) with 1 mM dNTP, 0.1 μg/μl BSA and 1 μM of the ID33 molecular beacon before Phi29 polymerase (1.5 nM, final concentration) was added. The samples were placed in the qPCR machine (Mx3000P, Agilent Technologies, Inc.) and incubated at 30°C for up to 4 h. The samples were analyzed by measuring FAM fluorescence emission over time (every 1 min) essentially as described in (59). Data from the run were processed in Microsoft Excel and unless stated otherwise, increases in fluorescence over time (as an estimate of reaction rate) were calculated from raw data generated between 80–120 min.

Microscopic readout

7.5 μl of samples containing released and nicked B-circle, prepared as described above, were mixed with 0.1 nM pre-

generated control circles. Then, the volume was adjusted to 10 μl of 1xRCA buffer (33 mM Tris-acetate, pH 7.9, 10 mM $MgCl_2$, 66 mM KCl, 1% (v/v) Tween 20 and 10 mM DTT) with 1 mM dNTP, 0.1 μg/μl BSA and 1 μM of the ID33 and ID16 molecular beacons with a FAM and CAL-Fluor-Red-590 (TAMRA analog) fluorophore, respectively, before Phi29 polymerase (1.5 nM, final concentration) was added to generate RCPs. The RCPs were hybridized to capture oligonucleotide printed Epoxy slides as described before (30,59). Finally, the slides were mounted with 2.5 μl Vectashield (Vector Laboratories) and a cover glass before analyses using the 63× objective of an Olympus IX73 fluorescence microscope. The pictures were exported from the fluorescent microscope software and analyzed by counting the fluorescent spots using ImageJ software (60). The number of green and red spots resulting from molecular beacon binding to RCPs generated from nicked B-circles and control circles, respectively, were calculated and the ratio between green and red signals (the green/red ratio) for each image were calculated. The mean of 12 images per experiment was determined. Mean green/red ratios from three experiments were normalized to show the fold-increase above the negative sample, by division with the mean of the negative.

Denaturing polyacrylamide gel electrophoresis

For the radioactively-labeled dsDNA catenane, oligonucleotide OL8 was 5′-labeled by T4 kinase by replacing non-labeled ATP with γ-P^{32}ATP and performing the 5′-phosphorylation reaction essentially as described above. The remaining oligonucleotides were cold phosphorylated and the catenane was assembled as described above. Samples from different steps (indicated in Figure 2A) in the assembly procedure were mixed with 1× loading buffer (80% (v/v) deionized formamide, 50 mM Tris borate (pH 8.3), 1 mM EDTA, 0.05% (w/v) bromophenol blue, and 0.05% (w/v) xylene xyanol), heated to 95°C for 2 min before analyzes in a 6% denaturing polyacrylamide gel. Radiolabeled DNA was visualized by radiography using a Personal Molecular Imager (Bio-Rad).

SDS-PAGE and western blotting

SDS-PAGE and western blots were performed essentially as described previously (61). Primary antibodies used were Rabbit monoclonal Anti-Topo IIα (ab52934, abcam), Rabbit polyclonal Anti-Topo IIβ (ab58442, abcam), Rabbit monoclonal Anti-GAPDH, (D16H11, Cell Signaling).

Decatenation assay

k-DNA (80 ng/μl, final concentration) was incubated with the indicated amount of purified Topo IIα or cell extract in 10 μl of 1xTopo II decatenation buffer (10 mM Tris–HCl pH 8, 10 mM $MgCl_2$, 0.5 mM EDTA, 15 μg/ml BSA, 100 mM KCl, 50 mM NaCl, 2% (v/v) glycerol and 1 mM ATP (unless stated otherwise)). After incubation at 37°C for 30 min, the reaction was terminated by the addition of SDS [1% (w/v), final concentration] before the samples were loaded on a 1% agarose gel, run for 1 h at 60 mA in 1xTBE buffer and analyzed by UV-light exposure after staining with ethidium bromide using a GelDoc (Biorad).

Competition assay involving Topo II suicide substrate

Topo II suicide substrate (described previously (62)) was prepared by allowing the two DNA oligonucleotides to hybridize in 1xTE (10 mM Tris–HCl, pH 7.5, 0.5 mM EDTA) by heating the sample to 95°C before slowly cooling down to room temperature. The suicide substrate (40 μM final) was added to the TADA-complex containing samples before the addition of nuclear extracts from 50 000 HeLa cells. As a control the suicide substrate was replaced by unspecific plasmid DNA (pUC18) that was added in the same amount (weight/volume) as the suicide substrate in one sample.

Multiplexing TADA and Topo I detection assay

After the final washing step of the TADA-complex (see above) the precipitated beads were re-suspended in Topo II decatenation buffer containing 1 nM S(Topo I). Purified Topo IIα (15 ng/μl, final concentration) and/or purified Topo I (2.5 ng/μl, final concentration) were added to the reaction mixtures containing both substrates as indicated in Figure 6. Samples were analyzed as described above, except that no control circles were added, instead 1 nM primer for RCA of S(hTopo I) circles was added prior to RCA. RCPs generated by RCA of nicked B-circle were visualized using the ID33 molecular beacon with a FAM fluorophore, while RCPs generated by RCA of the circularized S(Topo I) were visualized by the ID16 molecular beacon with a CAL-Fluor-Red-590 fluorophore. Hence, green fluorescence spots were counted as TADA specific signals, and red fluorescence spots were counted as Topo I specific signals.

Statistical analysis

All statistical analysis was carried out using unpaired, two tailed, student's t-tests (Prism 5.0, GraphPad Software, La Jolla, CA, USA).

RESULTS

Design of an RCA-based setup for detection of Topo II activity

To achieve specific detection of Topo II-catalyzed decatenation and avoid nonspecific reactions from DNA processing enzymes that are present in biological samples, we designed a small double-stranded DNA nanostructure composed of two interlinked DNA circles to act as a substrate for Topo II. This double-stranded DNA nanostructure is termed the dsDNA catenane (Figure 1A, Step 5). By lacking exposed DNA ends, the dsDNA catenane imitated undamaged genomic DNA and was anticipated to escape nonspecific degradation by exonucleases. The dsDNA catenane assembly was based on the formation of an intermediate single-stranded DNA catenane that was assembled by initial rounds of annealing between synthetic DNA oligonucleotides followed by ligation, where the sequences of the oligonucleotides ensured catenane formation (63). The single-stranded DNA catenane was converted

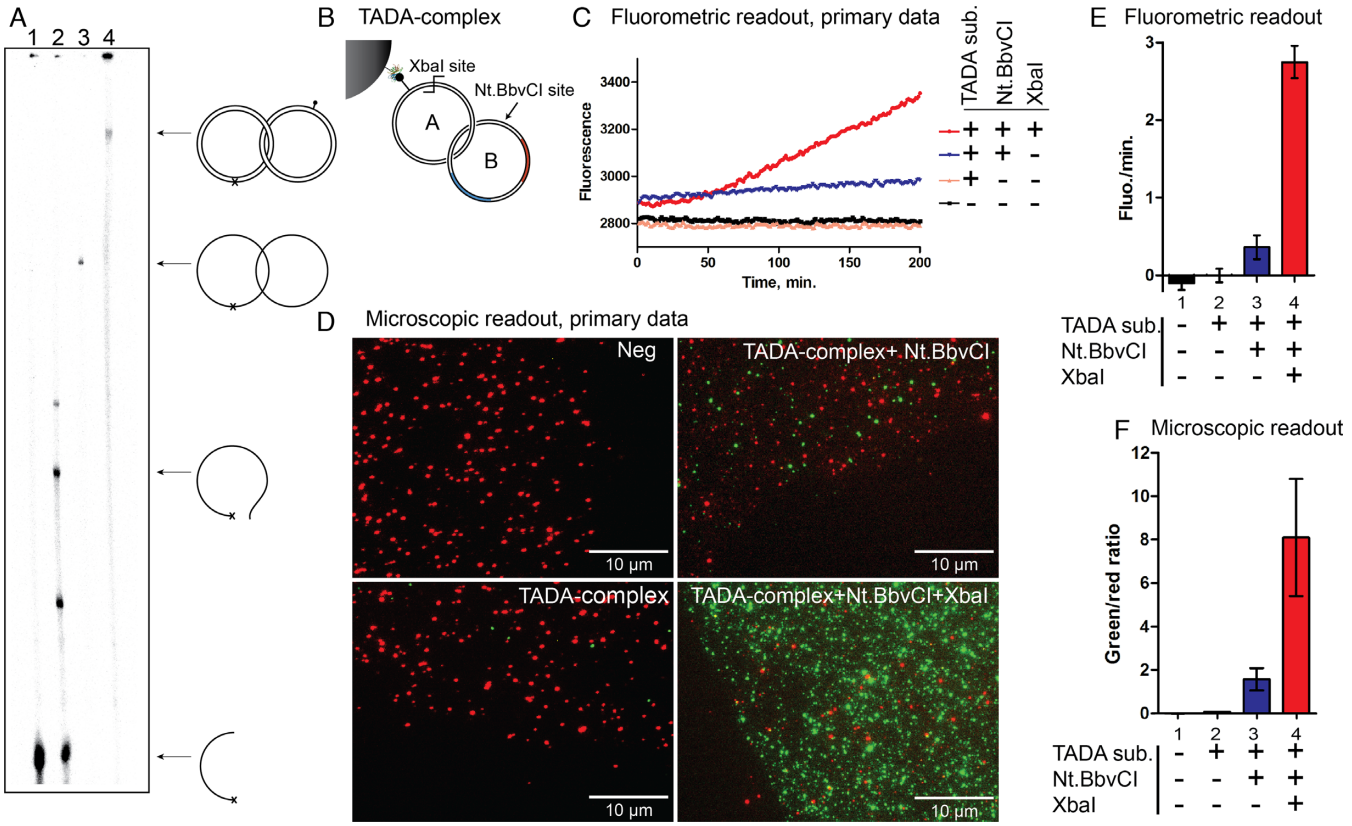

Figure 2. Validation of the TADA assembly. (**A**) Radiography of a 6% denaturing polyacrylamide gel in which products from different reaction steps in the assembly of the dsDNA catenane were analyzed. Lane 1, 120 nt radiolabeled oligonucleotide (OL8). Lane 2, products of ligation of OL8 (radiolabeled) and OL9 using OL11 as template. Lane 3, products obtained when the ligated product analyzed in Lane 2 were incubated with circularized A-circle followed by ligation and exonuclease treatment. Lane 4, products obtained when complementary oligonucleotides (OL4-OL7, OL10, OL12–16) were added to the reaction mixture analyzed in Lane 3 followed by ligation and exonuclease treatment. A schematic illustration of the expected products is shown to the right of the gel-picture. (**B**) Schematic illustration of the TADA-complex. The gray sphere represents the streptavidin coupled magnetic bead. The dsDNA catenane was bound to the bead through a biotin (black circle) internally inserted in the A-circle. The red segment on the B-circle represents the molecular beacon binding site. The blue segment represents the capture oligonucleotide binding site. (**C**) Representative example of primary results obtained when using the fluorometric readout, in which the TADA-complex has been treated with the indicated enzymes and the results detected in a fluorometer. (**D**) Representative example of results obtained when analyzing the same samples as the ones described in (C) using the microscopic readout. Red and green fluorescent spots represent RCPs generated from RCA of control circles and B-circles, respectively. Contrast and brightness have been adjusted for the images to improve image visualization. (**E**) Mean of the slopes (representing increase in fluorescence over time) calculated between 100–200 min from three test experiments analyzed by the fluorometric readout method. Error bars represent standard deviation (SD) of the slopes calculated from the three individual experiments. (**F**) Mean ratio between numbers of green and red spots (green/red ratio) calculated from multiple microscopic images ($n = 12$). Error bars represent the SD observed among the images in the experiment.

to a double-stranded catenane by the addition of complementary DNA oligonucleotides followed by an additional round of ligation (see Figure 1A, Steps 1–5). This resulted in the formation of a structure consisting of two interlinked double-stranded DNA circles, termed the A-circle and the B-circle of 221 and 220 bp, respectively (Figure 1A, Step 5). To allow coupling of the dsDNA catenane to streptavidin-coated magnetic beads, an internal biotin molecule (black circle in Figure 1A, Steps 4 and 5) was included in one of the oligonucleotides used during assembly. The attachment to magnetic beads allowed the removal of unreacted structures after incubation with Topo II and was a necessary step in the assay as illustrated in Figure 1B and explained below.

The dsDNA catenane was designed to allow enhanced detection of Topo II decatenation activity using a REEAD protocol. Reminiscent of REEAD assays specific for the simpler catalytic reactions of type IB topoisomerases, recombinases and integrases (39,40), this setup allowed single catalytic events mediated by Topo II (i.e. the complex decatenation reaction) to be converted to directly detectable signals. In Figure 1B, the workflow of the REEAD-based Topo II activity detection assay, termed TADA, is schematically illustrated. The experimental setup involves the following steps: (i) binding of the dsDNA catenane to streptavidin coated magnetic beads through the internal biotin to generate a TADA-complex, (ii) sample incubation during which a single B-circle is released from the TADA-complex by each decatenation event mediated by active Topo II, (iii) precipitation of magnetic beads and the addition of the nicking enzyme (Nt.BbvCI) specific for a DNA sequence present in the B-circle, leaving B-circles with single-stranded nicks and a free 3′-OH end in the supernatant, (iv) RCA of nicked B-circles primed by the 3′-OH group of the nick, followed by hybridization of the generated RCPs with molecular beacons (64), (v) detection in bulk samples using a fluorometer (termed fluorometric readout) or (vi) detection

at the single-RCP level using a fluorescence microscope after hybridization of end products to immobilized capture oligonucleotides (termed microscopic readout). Note that each fluorescent spot that is observed in the microscope corresponds to a single RCP (65), which in turn corresponds to a single released B-circle facilitated by a single decatenation event catalyzed by Topo II.

Assembly and quality test of the DNA nanostructure

A stepwise assembly experiment was performed in order to evaluate the dsDNA catenane formation (see details in Figure 1A). In the experimental setup, increasing numbers of DNA oligonucleotides (designed to form various parts of the catenane structure) were mixed and ligated and analyzed in a 6% denaturing polyacrylamide gel (Figure 2A). Products were visualized by radiolabeling one of the oligonucleotides (OL8) that was used for assembly. Lane 1 shows the mobility of radiolabeled OL8, which constituted one-half of the single-stranded B-circle. Upon mixing of this oligonucleotide with OL9 and OL11 (OL11 being the template for ligation between OL8 and OL9) and addition of ligase, a 220 nt product, corresponding to the single-stranded B-circle-forming strand, was created (see the product indicated by an arrow, lane 2 in Figure 2A). This radiolabeled 220 nt B-circle-forming strand was ligated to generate an exonuclease resistant single-stranded catenane upon addition of a pre-formed single-stranded A-circle (see lane 3 in Figure 2A). The dsDNA catenane was generated by the addition of oligonucleotides OL4–7, OL10, OL12–16 with sequences complementary to the sequences of the single-stranded catenane followed by ligation and exonuclease treatment (see lane 4 in Figure 2A). The appearance of a single exonuclease resistant product with a well-defined gel-electrophoretic mobility significantly slower than the mobility of the single-stranded catenane (compare lanes 3 and 4 in Figure 2A) suggested the generation of a fully assembled double-stranded catenane product. Some smear below the high mobility band in lane 4 could be observed. The identity of this smear is not clear although the lack of any specific bands in this smear may suggest that it is an artifact of running caused by impurities such as salt etc. in the analyzed samples.

The small size of the dsDNA catenane circles may inhibit enzymatic interactions with the DNA backbone. We therefore investigated whether the catenane circles could be unlinked by a model enzyme, restriction endonuclease, XbaI, and nicked by Nt.BbvCI. Note that nicking is necessary to create a 3′-OH end that can prime RCA of the B-circle and is, thus, an essential step for the TADA setup.

In the test experiments, the TADA-complex (which is the dsDNA catenane coupled to magnetic beads, illustrated in Figure 2B) was mixed with XbaI and/or Nt.BbvCI. After nuclease treatment, the magnetic beads were removed and RCA was performed as illustrated in Figure 1B (see Figure 1A for the position of the XbaI and Nt.BbvCI cleavage sites). Data were acquired by using fluorometric or microscopic readout. Primary results from the fluorometric readout are shown in Figure 2C and the calculated slopes of the increase in fluorescence over time are depicted in Figure 2E. Representative images from the microscopic readout are shown in Figure 2D and quantifications of the observed fluorescent spots representing RCPs generated in each sample are shown in Figure 2F. In this figure, the number of spots resulting from decatenation (green spots) or the addition of a known concentration of control circles (red spots) were counted for 12 images and the results depicted as the ratio between the number of green and red spots in the bar chart.

For both the fluorometric and microscopic readouts, a large increase in signals was observed upon the addition of XbaI and Nt.BbvCI to the TADA assay as compared to the addition of neither or only one of the endonucleases (see column 4 in Figures 2E and F). This suggests that unlinking of the B-circle and nicking support RCA as expected from the assay outline depicted in Figure 1B. The data also illustrate that the two readout methods can be used to detect the results form a single reaction mixture in either a quick convenient (fluorometric readout (20,64)) or a highly sensitive (microscopic readout (59,66)) manner. Note that in the sample with only Nt.BbvCI added, a small but consistent increase in signal compared to the sample with only TADA-complex was observed (compare columns 3 and 2 in Figures 2E and F). The reason for this is not fully understood. Most likely, this signal arose from a subpopulation of incorrectly assembled hemicatenated DNA structures that were released by Nt.BbvCI nicking and could be amplified using RCA. This explanation was indeed consistent with the lack of background signal observed when only XbaI was added strongly arguing against the background signals observed in column 3 being the result of nicked DNA circles (Supplementary Figure S1). The occurrence of background signals could be avoided by adding the unlinking enzyme activity (XbaI or Topo II) and the nicking enzyme (Nt.BbvCI) sequentially, interrupted by a bead precipitation step (data not shown). (This was done in the following experiments as described in materials and methods.) Consequently, such a protocol was followed in all experiments described below.

Quantitative detection of purified human Topo IIα activity by the TADA Setup

The results presented above demonstrate the ability of XbaI to cleave and unlink the dsDNA catenane. However, compared to XbaI, which simply cuts the DNA double helix, Topo II utilizes a decatenation reaction mechanism, which includes strong DNA bending as well as an orchestrated double-stranded opening and closing of a gate in the DNA (9,67,68). The ability of the TADA assay to measure the activity of Topo II in a quantitative manner was investigated by incubating the TADA-complex with decreasing concentrations of purified Topo IIα, which is one out of two isoforms of Topo II encoded by humans (41). Subsequently, released B-circles were separated from unreacted TADA-complexes before RCA, and microscopic detection of the resulting RCPs was performed as illustrated in Figure 1B. A quantitative relationship between the number of signals obtained and the concentration of Topo IIα was observed. The results are graphically depicted in Figure 3, while examples of the signals counted are shown in Supplementary Figure S2. The Topo IIα used in this experiment was purified from yeast. It appeared reasonably pure (see Supplementary Figure S3A) and its presence was confirmed by western blot-

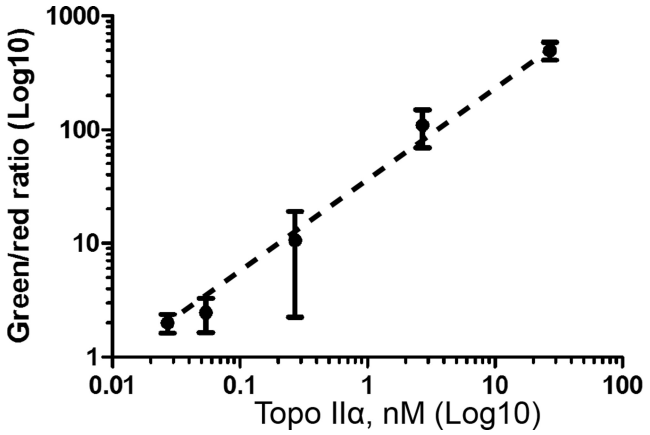

Figure 3. Detection of purified Topo IIα. Double logarithmic plot showing mean green/red ratios of triplicate experiments obtained when analyzing a titration of purified Topo IIα using the TADA. The TADA-complex was incubated with decreasing amounts of Topo IIα as noted in the figure and the results analyzed by the microscopic readout. Average amounts of green spots (TADA specific signals) and red spots (signals specific for added control circles) were calculated from 12 images from each experiment and used to calculate the plotted mean. Error bars represent SD from the mean green/red ratios from each of the three experiments.

ting (Figure 4A). Moreover, the decatenation activity was confirmed to originate from Topo IIα using a classical decatenation assay (69) performed with or without ATP (Supplementary Figure S3B and C).

Specific detection of Topo II in extracts from human cancer cells

The TADA setup was designed to be specific for Topo II in the presence of the complex mixture of enzymes in crude extracts from human cells. To investigate the specificity of the TADA experimentally, we compared the number of TADA signals observed in extracts from human cell lines that were either untreated or depleted for Topo II. As two mechanically similar isoforms of Topo II are expressed in human cells (41), both isoforms needed to be depleted in order to test the specificity of the assay. Attempts to deplete both enzymes in standard immuno-precipitation assays using commercially available antibodies failed. Instead Topo II depletion was accomplished by trapping the enzymes (both Topo IIα and Topo IIβ) on the genomic DNA by incubating the cell extracts with the Topo II poison, etoposide, which specifically stabilizes the Topo II-DNA cleavage complexes and thereby crosslink the enzymes to the genomic DNA (43,70,71). Subsequent precipitation of the genomic DNA together with the bound Topo II enzymes by centrifugation lead to a gentle yet specific depletion of both Topo IIα and Topo IIβ without denaturing the enzymes in the sample. The successful depletion of both Topo IIα and Topo IIβ by this method was demonstrated by western blot analysis using antibodies specific for each isoform (Figure 4A, compare lanes 1 and 2 in the top panel for Topo IIα depletion, and in the lower panel for Topo IIβ depletion). The Topo II-depleted or non-depleted cell extracts were incubated with the TADA-complex and their decatenation activities were analyzed. The results were compared to the decatenation activity of a heat-denatured cell extract chosen as a negative control to allow unspecific effects of proteins or other cellular components on the assay to be ruled out. To ensure maximum sensitivity, the microscopic readout was chosen for these experiments. As evident from Figure 4B, no significant difference in TADA generated signals was observed between the reactions incubated with Topo II-depleted cell extract (Topo II-dep) and the negative control (neg). In marked contrast, a large difference was observed when comparing results obtained with non-depleted (non-dep) and heat inactivated cell extracts. Taken together, the analysis of Topo II-depleted or non-depleted cell extracts strongly suggest that the TADA is specific for Topo II activity in human cell extracts. A similar result was obtained when analyzing the TADA signals generated by a HeLa cell extract incubated with the TADA-complex in the presence or absence of added ATP. As evident from Figure 4C the TADA signals generated by the added cell extract was significantly above the background signals generated in a sample incubated without added cell extract only in the presence of ATP (compare columns 1 and 2) and not in the absence of ATP (compare columns 3 and 4). Since Topo II decatenation strictly depend on ATP, while the potential decatenation activity of various endonucleases are independent of ATP this result strongly suggest that the TADA signals was generated specifically by Topo II acitivity in the cell extract.

The specificity of the TADA for Topo II activity was also confirmed by a competition experiment in which Topo II in cell extracts was specifically inhibited by the addition of a Topo II-specific so-called DNA suicide substrate (72) to the cell extract prior to mixing it with the TADA-complex. As illustrated in Figure 4D, the Topo II suicide substrate consists of two short oligonucleotides that hybridize to form a cleavage site for Topo II (72). The suicide substrate functions as a mechanism-based inhibitor of Topo II since the 3′-OH containing trinucleotide generated during cleavage dissociates from the substrate. This prevents the religation reaction and results in the accumulation of catalytically inert cleavage complexes (72). Consistent with the TADA being specific for Topo II activity, the TADA signal generated from a HeLa cell extract was significantly reduced upon addition of 40 μM DNA suicide substrate (Figure 4E, column 2) compared to the signal generated by a similar sample without added suicide substrate (Figure 4E, column 1). This decrease was not caused by the addition of DNA to the sample *per se*, as the addition of a similar amount (weight/volume) of plasmid DNA did not inhibit the generation of TADA signal. In fact, the addition of the plasmid DNA resulted in an increased signal compared to the signal generated in a sample where no DNA had been added. The reason for this increase is unclear, but it may be explained by increased access of Topo II to the TADA-complex due to less competition from other DNA binding enzymes, e.g. nucleases.

The detection limit of TADA in human cell extracts

As mentioned in the introduction, Topo II activity may be an important predictive marker for chemo-response in cancer patients. However, analyses of biopsies from patients are often hampered by limited sample size calling for hypersen-

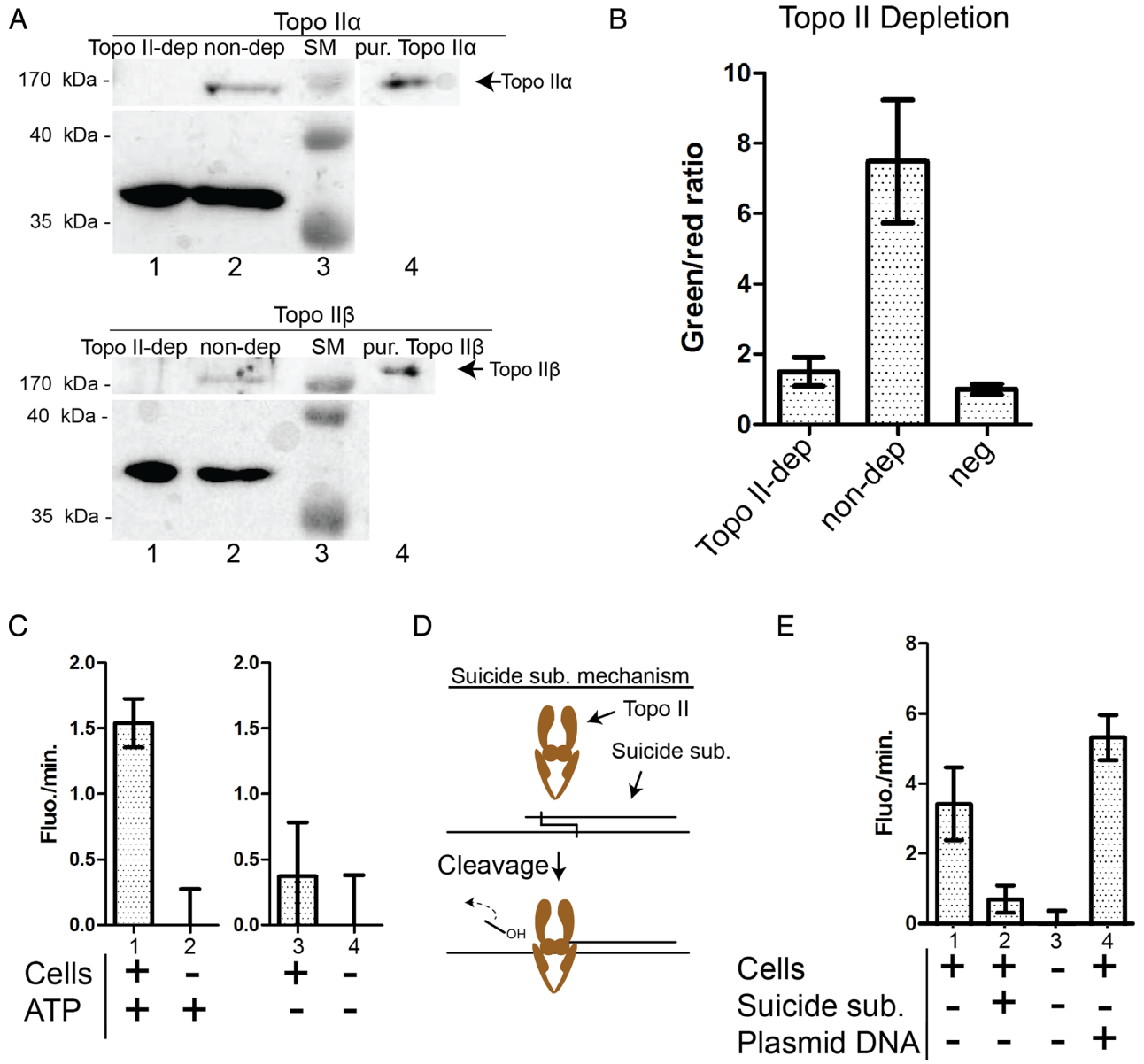

Figure 4. Analysis of the specificity of TADA in extracts from human cancer cells. (**A**) Western blot analysis of Topo II-depleted or non-depleted cell extracts. The upper panel shows western blots of the indicated sample types using an anti-human Topo IIα (170 kDa) antibody and an anti-glyceraldehyde-3-phosphate dehydrogenase (GAPDH) (37 kDa) antibody (as a loading control). Lane 1, Topo II-depleted cell extract; Lane 2, non-depleted cell extract; Lane 3, size marker; Lane 4, 200 ng of purified Topo IIα. Lower panel, same as upper panel, except that an anti-human Topo IIβ (180 kDa) antibody was used, and purified Topo IIβ was used as a loading control in Lane 4. (**B**) Bar chart of mean green/red ratios of triplicate experiments in which the TADA-complex was incubated with cell extracts either Topo II-depleted (Topo II-dep), or not depleted for Topo II (non-dep), or with heat inactivated non-depleted cell extract as a negative control (neg) before the results were analyzed using the microscopic readout. Error bars represent SD from mean green/red ratios calculated from 12 images per experiment repetition. (**C**) The results of incubating the TADA comples with or without a human cell extract in the presence of added ATP or in the absence of added ATP and indicated below the bar chart. The results were normalized by substrating the signals generated in the samples without added cell extracts. The error bars represent SD calculated from three experiments. (**D**) Schematic illustration of the Topo II-suicide substrate reaction by which Topo II was covalently bound to the suicide substrate after cleavage due to the dissociation of the 3′-OH end. (**E**) The result of a competition between the Topo II suicide reaction and the TADA. The bar chart shows the mean slopes calculated from triplicate experiments where the TADA-complex was incubated with cell extract, cell extract containing 40 μM suicide substrate, no cell extract, or cell extract containing pUC18 plasmid DNA (same amount (weight/volume) as the suicide substrate) and analyzed by TADA using the fluorometric readout. The error bars represent SD calculated from three experiments. The results were normalized by substrating the signals generated in the sample without added cell extracts.

sitive detection systems. To investigate the detection limit of the TADA setup, nuclear extracts from 5×10^4 HeLa cells were prepared and diluted as indicated in Figure 5. The Topo II activities in the diluted samples were measured in the TADA using the microscopic readout and the results are graphically depicted in Figure 5A. For comparison, similar samples were analyzed in a standard k-DNA decatenation assay in which decatenation activity was measured in terms of the gel-electrophoretic mobility of the products (Figure 5B). Note that k-DNA is the poly-catenated DNA genome from *kinetoplastida* mitochondria (69). Upon decatenation by Topo II, individual circles in the k-DNA are unlinked and can be separated from intact k-DNA using ultra-centrifugation or gel-electrophoreses (73), stained by intercalating dyes (e.g. SyBR green or EtBr) and quantified. From the result of the TADA titration experiment shown in Figure 5A, it is evident that significant detection of Topo II could be observed in extracts corresponding to as few as five cells. The signal resulting from incubation of the TADA-complex with extract diluted to a level corresponding to one cell was not different from the negative control without added cell extract within the standard deviation. A difference exceeding the standard deviation was, however, observed for signals resulting from incubation of the TADA complex with extracts corresponding to five cells or more. From these data it can be extrapolated that the detection limit of the TADA at the current reaction conditions will be within the interval corresponding to extract from two cells or more and five cells or less. This detection limit may even be improved by increasing e.g. the substrate concentration or the reaction time. Note, the current concentration of the TADA-complex was rather low (45 fmol). The traditional k-DNA decatenation assay (analyzed by gel-electrophoretic separation of k-DNA and released cirlces and subsequent EtBr staining) was approximately 100 times less sensitive than the TADA (see Figure 5B). This result demonstrates promise for the future use of the TADA for measuring Topo II activity in small biopsies from cancer patients. Note, that in order to boost the sensitivity of the k-DNA decatenation assay we used a large excess of substrate k-DNA resulting in saturation of the bands corresponding to the substrate in the slot of the gel after EtBr staining (Figure 5B, lanes 2–7). The loading of large quantities of k-DNA in the gel also resulted in the appearance of a week unspecific band with a mobility faster than the released monomeric circles even in the sample without added cell extract (lane 2). The slow mobility band evident in lane 7 was most probably caused by incomplete decatenation.

Multiplexed REEAD detection of human Topo IIα and Topo I

As previously demonstrated, REEAD assays can be multiplexed for simultaneous detection of two or more enzyme reactions (40). To illustrate that the TADA setup can be used in combination with other REEAD based assays, we combined detection of Topo II with the REEAD based detection of Topo I (30,40). Topo I is frequently targeted by chemotherapeutic drugs belonging to the camptothecin family such as topotecan and irinotecan, which are currently used in treatment of the colon-, ovaria and small-cell lung cancer (74,75). The available evidence suggests that the chemo-response of cancer cell lines are influenced by the activity level of Topo I (36). Tandem detection of Topo II and Topo I may be potentially interesting in relation to cancer description, prognosis, or prediction of drug response for e.g. future individualized cancer treatment.

Figure 6 shows the results of a multiplexing experiment in which the TADA-complex and the Topo I-dumbbell substrate for REEAD (termed S(Topo I)) were incubated with either purified Topo I (denoted 'I'), purified Topo IIα and Topo I (denoted 'I+II'), purified Topo IIα (denoted 'II'), or no enzyme (denoted 'neg'), followed by removal of magnetic beads, RCA amplification, and microscopic readout of the results. During RCA, two different molecular beacons specific for each of the generated RCPs were added to reaction mixtures, giving rise to green and red fluorescent spots representing signals generated by the Topo IIα and the Topo I activities, respectively. In the bar chart, the relative number of Topo IIα-TADA specific signals is represented by green bars and the relative number of Topo I-REEAD specific signals is illustrated by red bars. The obtained results demonstrate the possibilities of multiplexed detection of Topo II and Topo I present in the same sample using the RCA-based protocols. Due to a large difference in the total number of signals obtained when measuring Topo I and Topo II activities, the numbers were normalized as described in the figure legend before depiction. The non-normalized results can be seen in Supplementary Figure S4.

DISCUSSION

The current study demonstrates the usability of a double-stranded catenated DNA nanostructure composed of two interlinked DNA circles for the specific, quantitative, and highly sensitive detection of Topo II activity even in crude biological samples. Specificity was ensured by the composition of the nanostructure that served as a substrate for Topo II activity. Hence, the nanostructure was designed in such a way that the entity being detected, *i.e.* released double-stranded B-circle, could be generated by the decatenation activity of Topo II. Sensitivity was achieved by signal amplification *via* RCA, converting the decatenation reaction happening within nanometer dimensions to a micrometer sized RCP that was detectable at the single-molecule level using a fluorescence microscope. Due to the isothermal amplification protocol and the highly processive nature of the Phi29 polymerase used for RCP production, each generated RCP corresponded to a single released B-circle, which in turn corresponded to a single decatenation event. Hence, the described TADA protocol allowed Topo II activity to be detected at the single decatenation event level. Moreover, the method was directly quantitative in nature.

In line with these advantages using TADA, we demonstrated quantitative and specific detection of Topo II in human cell extract with an approximate 100 times improved sensitivity compared to the state-of-the-art k-DNA decatenation assay and a detection limit corresponding to the cellular content of Topo II in five HeLa cells or less. Fluorescence based sensor systems based on assays different than the traditional k-DNA decatenation assay for detection of Topo II activity have been reported. However, such systems

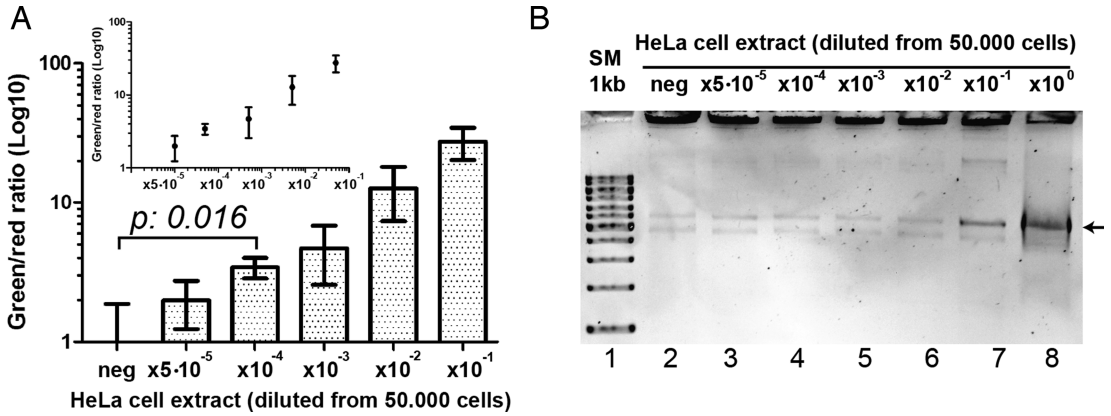

Figure 5. Determination of the detection limit of the TADA setup in cell extracts. (**A**) A Log_{10} bar chart showing mean green/red ratios calculated from triplicate TADA experiments using the microscopic readout. Nuclear cell extract was prepared from HeLa cells, and the extract diluted before the TADA activities were determined. The noted dilutions of HeLa cell extracts corresponded to extracts from 1 (5×10^{-5} dil.), 5 (10^{-4} dil.), 50 (10^{-3} dil.), 5×10^{2} (10^{-2} dil.), 5×10^{3} (10^{-1} dil.), 5×10^{4} (undil.) cells. The error bars represent SD from three individual experiments. The noted *P*-value (*P*: 0.016) was calculated using an unpaired two-tailed t-test. The inserted graph is a double logarithmic plot where the mean green/red ratios have been plotted as a function of number of cells analyzed. The dashed line indicates approximate linearity between signal observed and number of cells analyzed with the range of the dilution. (**B**) Representative 1% agarose gel image of a k-DNA decatenation experiment assaying the activity of the same cell extracts analyzed in (A). The arrow indicates the high mobility band resulting from Topo II decatenation of the k-DNA. A 1 kb size marker (SM) was loaded in Lane 1.

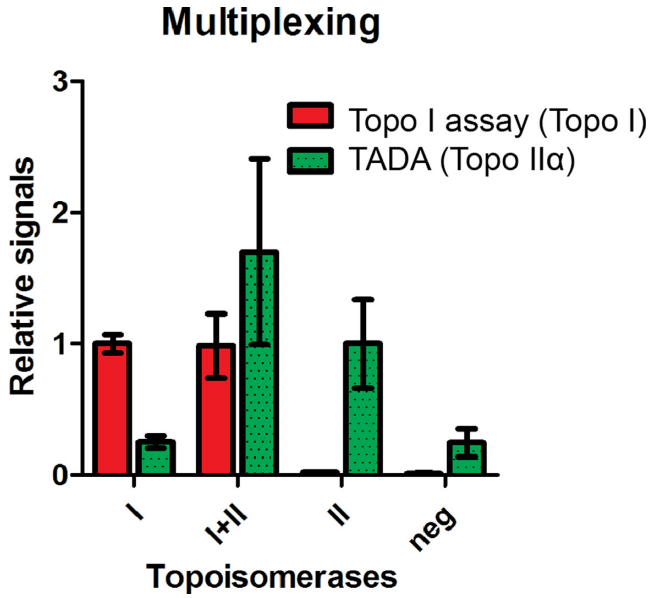

Figure 6. Multiplexed detection of Topo IIα and Topo I. The bar chart shows the results from triplicate experiments analyzed by the microscopic readout. The TADA-complex and the S(Topo I) were incubated with Topo I (noted as I), Topo IIα and Topo I (noted as I+II), Topo IIα (noted as II) or none of the enzymes (noted as neg) before RCA and readout. Green columns represent signals generated by TADA and red columns represent signals generated from the Topo I assay. Error bars represent SD from triplicate experiments. To enable display of the data in a single bar chart, the data were normalized by dividing the mean number of signals from the Topo I assay (red) or from the TADA (green) with the mean number of signals generated by analyzing purified Topo I or Topo IIα alone. Raw data without normalization are shown in Supplementary Figure S4.

have been based on the detection of non-Topo II-specific-reactions e.g. cleavage of double stranded DNA or relaxation of supercoiled plasmid DNA and can consequently only be used for measuring the activity of purified Topo II (76–78). In contrast, the TADA setup described here was specific for Topo II activity in crude human cell extracts as demonstrated by Topo II depletion and competition assays. As mentioned, Topo II is the cellular target of several clinically used anti-cancer drugs, which act by converting Topo II activity to a cell poison. Due to this mechanism of drug action Topo II activity is a potential marker for chemoresponse (54,79,80). Consistently, Topo II overexpression measured in terms of gene copy number, mRNA- or protein amount in tissue biopsies has been reported to correlate with the response on treatment with Topo II targeting drugs in breast cancer (52–56,81,82). However, enzyme activities are often regulated by mechanisms other than expression such as post-translational modifications or protein-protein interactions. Measurements of Topo II amount rather than activity may, therefore, be an unprecise marker for chemo-response. Such issues have not yet been addressed in part due to the lack of suitable assays. The described TADA presents the first tool for specific detection of Topo II with sufficient sensitivity for enzyme activity measurements in small clinical samples. This points toward a future use in basal as well as clinical science addressing the correlation between Topo II activity and chemoresponse and, ultimately, as a predictive tool in individualized cancer treatment. For such purposes, further developments should include the capacity to discriminate between the activities of Topo IIα and Topo IIβ (considered as having disproportional responsibilities for the cytotoxic and the genotoxic drug effects, respectively) (83–86), may be necessary. Such development can be envisioned by combining TADA with antibodies specific for each of the Topo II isoforms in an array format.

Moreover, multiplexed detection of Topo II activity with other cancer relevant enzyme activities in an RCA based setup as exemplified by multiplexed detection with Topo I in the current study may pave the road for development of platforms for comprehensive pre-treatment analyses of cancer biopsies.

SUPPLEMENTARY DATA

Supplementary Data are available at NAR Online.

ACKNOWLEDGEMENTS

We are grateful to Noriko Hansen for skillful technical assistance.

FUNDING

Familien Erichsens mindefond, Aase & Ejnar Danielsen's Foundation, Aage & Johanne Louis-Hansens Foundation, Marie & M.B. Richters Foundation, Minister Erna Hamiltons Legat for Videnskab og Kunst, Civilingeniør Frode V. Nyegaard og hustrus Fond, Karen Elise Jensens Foundation, Arvid Nilssons Foundation, Ludvid og Franciska Andersens legat, KUs Foundation for Cancer Research (to B.R.K.); Lundbeck Foundation (R95-A10275 to Y.P.H.); Arvid Nilssons Foundation; Chinese University of Hong Kong (CUHK) Start-up Fund and Research Direct Grant; NIH (GM033933 to N.O.). Funding for open access charge: Krista and Viggo Petersens Foundation.
Conflict of interest statement. None declared.

REFERENCES

1. Halder,S. and Krishnan,Y. (2015) Design of ultrasensitive DNA-based fluorescent pH sensitive nanodevices. *Nanoscale*, **7**, 10008–10012.
2. Brian R,Baker, Lai,R.Y., Wood,M.S., Doctor,E.H., Heeger,A.J. and Plaxco,K.W. (2006) An electronic, aptamer-based small-molecule sensor for the rapid, label-free detection of cocaine in adulterated samples and biological fluids. *J. Am. Chem. Soc.*, **128**, 3138–3139.
3. Zayats,M., Huang,Y., Gill,R., Ma,C.-A. and Willner,I. (2006) Label-free and reagentless aptamer-based sensors for small molecules. *J. Am. Chem. Soc.*, **128**, 13666–13667.
4. Liu,J., Wang,C., Jiang,Y., Hu,Y., Li,J., Yang,S., Li,Y., Yang,R., Tan,W. and Huang,C.Z. (2013) Graphene signal amplification for sensitive and real-time fluorescence anisotropy detection of small molecules. *Anal. Chem.*, **85**, 1424–1430.
5. Bi,S., Li,L. and Zhang,S. (2010) Triggered polycatenated DNA scaffolds for DNA sensors and aptasensors by a combination of rolling circle amplification and DNAzyme amplification. *Anal. Chem.*, **82**, 9447–9454.
6. Zuccaro,L., Tesauro,C., Kurkina,T., Fiorani,P., Yu,H.K., Knudsen,B.R., Kern,K., Desideri,A. and Balasubramanian,K. (2015) Real-time label-free direct electronic monitoring of topoisomerase enzyme binding kinetics on graphene. *ACS Nano*, **9**, 11166–11176.
7. Jensen,P.W., Falconi,M., Kristoffersen,E.L., Simonsen,A.T., Cifuentes,J.B., Marcussen,L.B., Frøhlich,R., Vagner,J., Harmsen,C., Juul,S. *et al.* (2013) Real-time detection of TDP1 activity using a fluorophore-quencher coupled DNA-biosensor. *Biosens. Bioelectron.*, **48**, 230–237.
8. Kristoffersen,E.L., Jørgensen,L.A., Franch,O., Etzerodt,M., Frøhlich,R., Bjergbæk,L., Stougaard,M., Ho,Y.-P. and Knudsen,B.R. (2015) Real-time investigation of human topoisomerase I reaction kinetics using an optical sensor: a fast method for drug screening and determination of active enzyme concentrations. *Nanoscale*, **7**, 9825–9834.
9. Hardin,A.H., Sarkar,S.K., Seol,Y., Liou,G.F., Osheroff,N. and Neuman,K.C. (2011) Direct measurement of DNA bending by type IIA topoisomerases: implications for non-equilibrium topology simplification. *Nucleic Acids Res.*, **39**, 5729–5743.
10. Jepsen,M.L., Harmsen,C., Godbole,A.A., Nagaraja,V., Knudsen,B.R. and Ho,Y.-P. (2016) Specific detection of the cleavage activity of mycobacterial enzymes using a quantum dot based DNA nanosensor. *Nanoscale*, **8**, S1–S2.
11. Goodman,R.P., Heilemann,M., Doose,S., Erben,C.M., Kapanidis,A.N. and Turberfield,A.J. (2008) Reconfigurable, braced, three-dimensional DNA nanostructures. *Nat. Nanotechnol.*, **3**, 93–96.
12. Banerjee,A., Bhatia,D., Saminathan,A., Chakraborty,S., Kar,S. and Krishnan,Y. (2013) Controlled release of encapsulated cargo from a DNA icosahedron using a chemical trigger. *Angew. Chem. Int. Ed.*, **52**, 6854–6857.
13. Juul,S., Iacovelli,F., Falconi,M., Kragh,S.L., Christensen,B., Frøhlich,R., Franch,O., Kristoffersen,E.L., Stougaard,M., Leong,K.W. *et al.* (2013) Temperature-controlled encapsulation and release of an active enzyme in the cavity of a self-assembled DNA nanocage. *ACS Nano*, **7**, 9724–9734.
14. Takenaka,T., Endo,M., Suzuki,Y., Yang,Y., Emura,T., Hidaka,K., Kato,T., Miyata,T., Namba,K. and Sugiyama,H. (2014) Photoresponsive DNA nanocapsule having an open/close system for capture and release of nanomaterials. *Chemistry*, **20**, 14951–14954.
15. Fujita,H., Kataoka,Y., Tobita,S., Kuwahara,M. and Sugimoto,N. (2016) Novel one-tube-one-step real-time methodology for rapid transcriptomic biomarker detection: signal amplification by ternary initiation complexes. *Anal Chem.*, **88**, 7137–7144.
16. Jacobsen,M.F., Ravnsbæk,J.B., Gothelf,K. V., Hannon,M.J., Chaires,J.B., Ren,J., Henary,M., Zegrocka,O., Bishop,G.R., Strekowski,L. *et al.* (2010) Small molecule induced control in duplex and triplex DNA-directed chemical reactions. *Org. Biomol. Chem.*, **8**, 50–52.
17. Mignardi,M., Mezger,A., Qian,X., La Fleur,L., Botling,J., Larsson,C. and Nilsson,M. (2015) Oligonucleotide gap-fill ligation for mutation detection and sequencing in situ. *Nucleic Acids Res.*, **43**, e151.
18. Kühnemund,M., Hernández-Neuta,I., Sharif,M.I., Cornaglia,M., Gijs,M.A.M. and Nilsson,M. (2017) Sensitive and inexpensive digital DNA analysis by microfluidic enrichment of rolling circle amplified single-molecules. *Nucleic Acids Res.*, doi:10.1093/nar/gkw1324.
19. Krzywkowski,T., Hauling,T. and Nilsson,M. (2017) In situ single-molecule RNA genotyping using padlock probes and rolling circle amplification. *Methods Mol. Biol.*, **1492**, 59–76.
20. Nilsson,M., Gullberg,M., Dahl,F., Szuhai,K. and Raap,A.K. (2002) Real-time monitoring of rolling-circle amplification using a modified molecular beacon design. *Nucleic Acids Res.*, **30**, 1–7.
21. Lohmann,J.S., Stougaard,M. and Koch,J. (2007) Detection of short repeated genomic sequences on metaphase chromosomes using padlock probes and target primed rolling circle DNA synthesis. *BMC Mol. Biol.*, **8**, 103.
22. Larsson,C., Koch,J., Nygren,A., Janssen,G., Raap,A.K., Landegren,U. and Nilsson,M. (2004) In situ genotyping individual DNA molecules by target-primed rolling-circle amplification of padlock probes. *Nat. Methods*, **1**, 227–232.
23. Baner,J., Nilsson,M., Mendel-Hartvig,M. and Landegren,U. (1998) Signal amplification of padlock probes by rolling circle replication. *Nucleic Acids Res.*, **26**, 5073–5078.
24. Cho,E.J., Yanq,L., Lew,M. and Ellinqton,A.D. (2005) Using a deoxyribozyme ligase and rolling circle amplification to detect a non-nucleic acid analyte, ATP. *J. Am. Chem. Soc.*, **127**, 2022–2023.
25. Ma,C., Wang,W., Yang,Q., Shi,C. and Cao,L. (2011) Cocaine detection via rolling circle amplification of short DNA strand separated by magnetic beads. *Biosens. Bioelectron.*, **26**, 3309–3312.
26. Zhao,W., Ali,M.M., Brook,M.A. and Li,Y. (2008) Rolling circle amplification: applications in nanotechnology and biodetection with functional nucleic acids. *Angew. Chem. Int. Ed. Engl.*, **47**, 6330–6337.
27. Monsur Ali,M. and Li,Y. (2009) Colorimetric sensing by using allosteric-DNAzyme-coupled rolling circle amplification and a peptide nucleic acid-organic dye probe. *Angew. Chem. Int. Ed.*, **48**, 3512–3515.
28. Lizardi,P.M., Ward,D.C., Huang,X., Zhu,Z., Bray-Ward,P. and Thomas,D.C. (1998) Mutation detection and single-molecule counting using isothermal rolling-circleamplification. *Nat. Genet.*, **19**, 225–232.
29. Blab,G.A., Schmidt,T. and Nilsson,M. (2004) Homogeneous detection of single rolling circle replication products. *Anal. Chem.*, **76**, 495–498.
30. Stougaard,M., Lohmann,J.S., Mancino,A., Celik,S., Andersen,F.F., Koch,J. and Knudsen,B.R. (2009) Single-molecule detection of human topoisomerase I cleavage-ligation activity. *ACS Nano*, **3**, 223–233.

31. Mizuta,R., Mizuta,M. and Kitamura,D. (2003) Atomic force microscopy analysis of rolling circle amplification of plasmid DNA. *Arch. Histol. Cytol.*, **66**, 175–181.
32. Cheglakov,Z., Weizmann,Y., Basnar,B. and Willner,I. (2007) Diagnosing viruses by the rolling circle amplified synthesis of DNAzymes. *Org. Biomol. Chem.*, **5**, 223–225.
33. Akhtar,S., Strömberg,M., Zardán Gómez de la Torre,T., Russell,C., Gunnarsson,K., Nilsson,M., Svedlindh,P., Strømme,M. and Leifer,K. (2010) Real-space transmission electron microscopy investigations of attachment of functionalized magnetic nanoparticles to DNA-coils acting as a biosensor. *J. Phys. Chem. B*, **114**, 13255–13262.
34. Cheng,W., Yan,F., Ding,L., Ju,H. and Yin,Y. (2010) Cascade signal amplification strategy for subattomolar protein detection by rolling circle amplification and quantum dots tagging. *Anal. Chem.*, **82**, 3337–3342.
35. Juul,S., Ho,Y.-P., Stougaard,M., Koch,J., Andersen,F.F., Leong,K.W. and Knudsen,B.R. (2011) Microfluidics-mediated isothermal detection of enzyme activity at the single molecule level. *Conf. Proc. IEEE Eng. Med. Biol. Soc.*, **2011**, 3258–3261.
36. Roy,A., Tesauro,C., Frøhlich,R., Hede,M.S., Nielsen,M.J., Kjeldsen,E., Bonven,B., Stougaard,M., Gromova,I. and Knudsen,B.R. (2014) Decreased camptothecin sensitivity of the stem-cell-like fraction of caco2 cells correlates with an altered phosphorylation pattern of topoisomerase I. *PLoS One*, **9**, e99628.
37. Tesauro,C., Juul,S., Arno,B., Nielsen,C.J.F., Fiorani,P., Frohlich,R.F., Andersen,F.F., Desideri,A., Stougaard,M., Petersen,E. *et al.* (2012) Specific detection of topoisomerase i from the malaria causing P. falciparum parasite using isothermal Rolling Circle Amplification. In: *Proceedings of the Annual International Conference of the IEEE Engineering in Medicine and Biology Society*, EMBS. pp. 2416–2419.
38. Juul,S., Nielsen,C.J.F., Labouriau,R., Roy,A., Tesauro,C., Jensen,P.W., Harmsen,C., Kristoffersen,E.L., Chiu,Y.-L., Frøhlich,R. *et al.* (2012) Droplet microfluidics platform for highly sensitive and quantitative detection of malaria-causing Plasmodium parasites based on enzyme activity measurement. *ACS Nano*, **6**, 10676–10683.
39. Wang,J., Liu,J., Thomsen,J., Selnihhin,D., Hede,M.S., Kirsebom,F.C.M., Franch,O., Fjelstrup,S., Stougaard,M., Ho,Y.-P. *et al.* (2017) Novel DNA sensor system for highly sensitive and quantitative retrovirus detection using virus encoded integrase as a biomarker. *Nanoscale*, **4**, e5819.
40. Andersen,F.F., Stougaard,M., Jørgensen,H.L., Bendsen,S., Juul,S., Hald,K., Andersen,A.H., Koch,J. and Knudsen,B.R. (2009) Multiplexed detection of site specific recombinase and DNA topoisomerase activities at the single molecule level. *ACS Nano*, **3**, 4043–4054.
41. Champoux,J.J. (2001) DNA topoisomerases: structure, function, and mechanism. *Annu. Rev. Biochem.*, **70**, 369–413.
42. Nitiss,J.L. (2009) Targeting DNA topoisomerase II in cancer chemotherapy. *Nat. Rev. Cancer*, **9**, 338–350.
43. Deweese,J.E. and Osheroff,N. (2009) The DNA cleavage reaction of topoisomerase II: wolf in sheep's clothing. *Nucleic Acids Res.*, **37**, 738–748.
44. Tan,T.C., Bouras,S., Sawaya,H., Sebag,I.A., Cohen,V., Picard,M.H., Passeri,J., Kuter,I. and Scherrer-Crosbie,M. (2015) Time trends of Lleft ventricular ejection fraction and myocardial deformation indices in a cohort of women with breast cancer treated with anthracyclines, taxanes, and trastuzumab. *J. Am. Soc. Echocardiogr.*, **28**, 509–514.
45. von Pawel,J., Jotte,R., Spigel,D.R., O'Brien,M.E.R., Socinski,M.A., Mezger,J., Steins,M., Bosquee,L., Bubis,J., Nackaerts,K. *et al.* (2014) Randomized phase III trial of amrubicin versus topotecan as second-line treatment for patients with small-cell lung cancer. *J. Clin. Oncol.*, **32**, 4012–4019.
46. Ezoe,S. (2012) Secondary leukemia associated with the anti-cancer agent, etoposide, a topoisomerase II inhibitor. *Int. J. Environ. Res. Public Health*, **9**, 2444–2453.
47. Henderson,T.O., Rajaraman,P., Stovall,M., Constine,L.S., Olive,A., Smith,S.A., Mertens,A., Meadows,A., Neglia,J.P., Hammond,S. *et al.* (2012) Risk factors associated with secondary sarcomas in childhood cancer survivors: a report from the childhood cancer survivor study. *Int. J. Radiat. Oncol.*, **84**, 224–230.
48. Pendleton,M., Lindsey,R.H., Felix,C.A., Grimwade,D. and Osheroff,N. (2014) Topoisomerase II and leukemia. *Ann. N. Y. Acad. Sci.*, **1310**, 98–110.
49. Wang,J.C. (2002) Cellular roles of DNA topoisomerases: a molecular perspective. *Nat .Rev. Mol. Cell. Biol.*, **3**, 430–440.
50. Wendorff,T.J., Schmidt,B.H., Heslop,P., Austin,C.A. and Berger,J.M. (2012) The structure of DNA-bound human topoisomerase II alpha: Conformational mechanisms for coordinating inter-subunit interactions with DNA cleavage. *J. Mol. Biol.*, **424**, 109–124.
51. Berger,J.M., Gamblin,S.J., Harrison,S.C. and Wang,J.C. (1996) Structure and mechanism of DNA topoisomerase II. *Nature*, **379**, 225–232.
52. Wang,J., Xu,B., Yuan,P., Zhang,P., Li,Q., Ma,F. and Fan,Y. (2012) TOP2A amplification in breast cancer is a predictive marker of anthracycline-based neoadjuvant chemotherapy efficacy. *Breast Cancer Res. Treat.*, **135**, 531–537.
53. Nielsen,K.V., Ejlertsen,B., Møller,S., Jørgensen,J.T., Knoop,A., Knudsen,H. and Mouridsen,H.T. (2008) The value of TOP2A gene copy number variation as a biomarker in breast cancer: Update of DBCG trial 89D. *Acta Oncol.*, **47**, 725–734.
54. Knoop,A.S., Knudsen,H., Balslev,E., Rasmussen,B.B., Overgaard,J., Nielsen,K.V, Schonau,A., Gunnarsdóttir,K., Olsen,K.E., Mouridsen,H. *et al.* (2005) retrospective analysis of topoisomerase IIa amplifications and deletions as predictive markers in primary breast cancer patients randomly assigned to cyclophosphamide, methotrexate, and fluorouracil or cyclophosphamide, epirubicin, and fluorouracil: Danis. *J. Clin. Oncol.*, **23**, 7483–7490.
55. Callagy,G., Pharoah,P., Chin,S.-F., Sangan,T., Daigo,Y., Jackson,L. and Caldas,C. (2005) Identification and validation of prognostic markers in breast cancer with the complementary use of array-CGH and tissue microarrays. *J. Pathol.*, **205**, 388–396.
56. Brase,J.C., Schmidt,M., Fischbach,T., Sültmann,H., Bojar,H., Koelbl,H., Hellwig,B., Rahnenführer,J., Hengstler,J.G. and Gehrmann,M.C. (2010) ERBB2 and TOP2A in breast cancer: A comprehensive analysis of gene amplification, RNA levels, and protein expression and their influence on prognosis and prediction. *Clin. Cancer Res.*, **16**, 2391–2401.
57. Kingma,P.S., Greider,C.A. and Osheroff,N. (1997) Spontaneous DNA lesions poison human Topoisomerase IIalpha and stimulate cleavage proximal to leukemic 11q23 chromosomal breakpoints. *Biochemistry*, **36**, 5934–5939.
58. Wang,Y., Thyssen,A., Westergaard,O. and Andersen,A.H. (2000) Position-specific effect of ribonucleotides on the cleavage activity of human topoisomerase II. *Nucleic Acids Res.*, **28**, 4815–4821.
59. Givskov,A., Kristoffersen,E., Vandsø,K., Ho,Y.-P., Stougaard,M. and Knudsen,B. (2016) Optimized detection of Plasmodium falciparum topoisomerase I enzyme activity in a complex biological sample by the use of molecular beacons. *Sensors*, **16**, 1916.
60. Schneider,C.A., Rasband,W.S. and Eliceiri,K.W. (2012) NIH Image to ImageJ: 25 years of image analysis. *Nat. Methods*, **9**, 671–675.
61. Hede,M.S., Petersen,R.L., Frøhlich,R.F., Krüger,D., Andersen,F.F., Andersen,A.H. and Knudsen,B.R. (2007) Resolution of Holliday junction substrates by human topoisomerase I. *J. Mol. Biol.*, **365**, 1076–1092.
62. Anderson,A.H., Sørensen,B.S., Christiansen,K., Svejstrup,J.Q., Lund,K. and Westergaard,O. (1991) Studies of the topoisomerase II-mediated cleavage and religation reactions by use of a suicidal double-stranded DNA substrate. *J. Biol. Chem.*, **266**, 9203–10.
63. Billen,L.P. and Li,Y. (2004) Synthesis and characterization of topologically linked single-stranded DNA rings. *Bioorg. Chem.*, **32**, 582–598.
64. Kristoffersen,E.L., Gonzalez,M., Stougaard,M. and Tesauro,C. (2014) Molecular beacon enables combination of highly processive and highly sensitive rolling circle amplification readouts for detection of DNA-modifying enzymes. *Nano Life*, doi:10.1142/S1793984415410020.
65. Stougaard,M., Juul,S., Andersen,F.F. and Knudsen,B.R. (2011) Strategies for highly sensitive biomarker detection by Rolling Circle Amplification of signals from nucleic acid composed sensors. *Integr. Biol.*, **3**, 982.
66. Lizardi,P.M., Huang,X., Zhu,Z., Bray-Ward,P., Thomas,D.C. and Ward,D.C. (1998) Mutation detection and single-molecule counting using isothermal rolling-circle amplification. *Nat. Genet.*, **19**, 225–232.
67. Redinbo,M.R., Stewart,L., Kuhn,P., Champoux,J.J. and Hol,W.G. (1998) Crystal structures of human topoisomerase I in covalent and noncovalent complexes with DNA. *Science*, **279**, 1504–1513.

68. Imsang Lee,K.C.D.J.M.B. (2013) The role of DNA bending in type IIA topoisomerase function. *Nucleic Acids Res.*, **41**, 5444.
69. Marini,J.C., Miller,K.G. and Englund,P.T. (1980) Decatenation of kinetoplast DNA by topoisomerases. *J. Biol. Chem.*, **255**, 4976–4979.
70. Ross,W., Rowe,T., Glisson,B., Yalowich,J. and Liu,L. (1984) Role of topoisomerase II in mediating epipodophyllotoxin-induced DNA cleavage. *Cancer Res.*, **44**, 5857–5860.
71. Tewey,K.M., Rowe,T.C., Yang,L., Halligan,B.D. and Liu,L.F. (1984) Adriamycin-induced DNA damage mediated by mammalian DNA topmoisomerase II. *Science (New York, NY)*, **226**, 466–468.
72. Sørensen,B.S., Sinding,J., Andersen,A.H., Alsner,J., Jensen,P.B. and Westergaard,O. (1992) Mode of action of topoisomerase II-targeting agents at a specific DNA sequence. Uncoupling the DNA binding, cleavage and religation events. *J. Mol. Biol.*, **228**, 778–786.
73. Mudeppa,D.G., Kumar,S., Kokkonda,S., White,J. and Rathod,P.K. (2015) Topoisomerase II from human malaria parasites: Expression, purification, and selective inhibition. *J. Biol. Chem.*, **290**, 20313–20324.
74. Hsiang,Y.H. and Liu,L.F. (1988) Identification of mammalian DNA topoisomerase I as an intracellular target of the anticancer drug camptothecin. *Cancer Res.*, **48**, 1722–1726.
75. Kiselev,E., Sooryakumar,D., Agama,K., Cushman,M. and Pommier,Y. (2014) Optimization of the lactam side chain of 7-azaindenoisoquinoline topoisomerase I inhibitors and mechanism of action studies in cancer cells. *J. Med. Chem.*, **57**, 1289–1298.
76. Shapiro,A.B. (2013) A high-throughput-compatible, fluorescence anisotropy-based assay for ATP-dependent supercoiled DNA relaxation by human topoisomerase IIα. *Biochem. Pharmacol.*, **85**, 1269–1277.
77. Jahnz,M., Medina,M.A. and Schwille,P. (2005) A novel homogenous assay for topoisomerase II action and inhibition. *Chembiochem.*, **6**, 920–926.
78. Shapiro,A.B. and Austin,C.A. (2014) A high-throughput fluorescence anisotropy-based assay for human topoisomerase II β-catalyzed ATP-dependent supercoiled DNA relaxation. *Anal. Biochem.*, **448**, 23–29.
79. Baldwin,E.L. and Osheroff,N. (2005) Etoposide, topoisomerase II and cancer. *Curr. Med. Chem. Agents*, **5**, 363–372.
80. Lynch,B.J., Guinee,D.G. and Holden,J.A. (1997) Human DNA topoisomerase II-alpha: a new marker of cell proliferation in invasive breast cancer. *Hum. Pathol.*, **28**, 1180–1188.
81. Durbecq,V., Paesmans,M., Cardoso,F., Desmedt,C., Di Leo,A., Chan,S., Friedrichs,K., Pinter,T., Van Belle,S., Murray,E. *et al.* (2004) Topoisomerase-II alpha expression as a predictive marker in a population of advanced breast cancer patients randomly treated either with single-agent doxorubicin or single-agent docetaxel. *Mol. Cancer Ther.*, **3**, 1207–1214.
82. Nakopoulou,L., Lazaris,A.C., Kavantzas,N., Alexandrou,P., Athanassiadou,P., Keramopoulos,A. and Davaris,P. (2000) DNA topoisomerase II-alpha immunoreactivity as a marker of tumor aggressiveness in invasive breast cancer. *Pathobiology*, **68**, 137–143.
83. Azarova,A.M., Lyu,Y.L., Lin,C.-P., Tsai,Y.-C., Lau,J.Y.-N., Wang,J.C. and Liu,L.F. (2007) Roles of DNA topoisomerase II isozymes in chemotherapy and secondary malignancies. *Proc. Natl. Acad. Sci. U.S.A.*, **104**, 11014–11019.
84. Haffner,M.C., Aryee,M.J., Toubaji,A., Esopi,D.M., Albadine,R., Gurel,B., Isaacs,W.B., Bova,G.S., Liu,W., Xu,J. *et al.* (2010) Androgen-induced TOP2B-mediated double-strand breaks and prostate cancer gene rearrangements. *Nat. Genet.*, **42**, 668–675.
85. Lyu,Y.L., Kerrigan,J.E., Lin,C.-P., Azarova,A.M., Tsai,Y.-C., Ban,Y. and Liu,L.F. (2007) Topoisomerase IIbeta mediated DNA double-strand breaks: implications in doxorubicin cardiotoxicity and prevention by dexrazoxane. *Cancer Res.*, **67**, 8839–8846.
86. Vejpongsa,P. and Yeh,E.T.H. (2014) Topoisomerase 2β: a promising molecular target for primary prevention of anthracycline-induced cardiotoxicity. *Clin. Pharmacol. Ther.*, **95**, 45–52.